22nd International Conference on Sustainable Energy Technologies
Kuala Lumpur, Malaysia, 13 to 15 August 2026 · ISBN 978-1-995850-00-9 · ISSN 2978-4387

CONFERENCE PAPER · ENERGY STORAGE & CONVERSION

Design and performance analysis of a CO_2 heat pump thermal storage system decoupled from a coal-fired power plant

Tengjiao Jia[1], Wen Su[1]*, Xinxing Lin[2], Zhimei Zheng[2]

[1] School of Energy Science and Engineering, Central South University, Changsha, Hunan, China
[2] Institute of Science and Technology, China Three Gorges Corporation, Beijing, China

RECEIVED 11 April 2026 · REVISED 11 May 2026 · ACCEPTED 21 May 2026
PRESENTED 13 to 15 August 2026 · PUBLISHED 23 November 2026

ABSTRACT

To address the intermittency of renewable energy and enhance renewable energy integration, a CO_2 heat pump thermal energy storage system decoupled from a coal-fired power plant (CFPP) was proposed. Taking a 600 MW supercritical CFPP in Dalian, China as a case study, a low-temperature water storage subsystem was introduced by utilizing fifth-stage low-pressure extraction steam, enabling the decoupling of CFPP and heat pump operations. The stored low-grade heat was subsequently upgraded by a CO_2 heat pump and transferred to a molten-salt thermal energy storage system using surplus electricity from the CFPP or renewable energy sources. Based on this configuration, three charging strategies were realized, including standalone steam extraction thermal storage, standalone heat pump thermal storage, and their combined operation. Results showed that, under the 30% turbine heat acceptance (THA) charging condition, standalone steam extraction reduced the minimum operating load to 29.72% THA, while the combined operation mode further decreased it to 12.16% THA after 8 h of heat storage. During the discharging process, the molten salt storage system effectively increased the CFPP output, raising the operating load to 43.13%, 65.24%, 91.60%, and 117.18% THA under baseline loads of 30%, 50%, 75%, and 100% THA, respectively, without exceeding safe turbine operating limits. The corresponding power generation efficiency ranged from 33.98% to 45.15%, while the round-trip efficiency (RTE) varied between 44.29% and 58.09%. Under the reference operating condition of 30% THA charging and 50% THA discharging, the CO_2 heat pump achieved a coefficient of performance (COP) of 1.32, and the overall system attained an RTE of 53.41%. The required volumes of the molten-salt storage tanks and storage water pools were 5.68×10^3 m^3 and 7.73×10^3 m^3, respectively. The results demonstrated that the proposed system could significantly extend the peak-shaving range of CFPPs and improve their adaptability to renewable energy fluctuations, providing a promising pathway for flexible operation and renewable energy accommodation.

KEYWORDS CFPP, CO_2 heat pump, Thermal energy storage, Thermodynamic analysis

1. Introduction

Nowadays, the rapid deployment of renewable energy accelerated the transition toward carbon-neutral energy systems. However, the intermittent and fluctuating nature of wind and solar power increased the mismatch between electricity supply and demand, creating growing requirements for grid flexibility and large-scale energy storage technologies (International Energy Agency 2024a; International Energy Agency 2024b; Dunn *et al.* 2011; Luo *et al.* 2015). At the same time, coal-fired power plants (CFPPs) still accounted for a significant share of electricity generation in many countries and were increasingly required to provide peak-shaving and load-following services rather than operating solely at base load (Liu *et al.* 2025). Nevertheless, conventional CFPPs were designed

* Corresponding author. Email address: suwenzn@csu.edu.cn (Wen Su)

© 2026 The Author(s).
Published by Caravel Press.

doi.org/10.65582/set.2026.006

for stable operation near rated conditions, and frequent deep-load regulation might result in efficiency degradation, increased fuel consumption, and operational constraints (Xu *et al.* 2025; Fang *et al.* 2025). Therefore, integrating energy storage systems with CFPPs was widely regarded as an effective approach to improve operational flexibility and facilitate renewable energy integration (Richter *et al.* 2019; Zhang *et al.* 2022a).

Among various technologies, thermal energy storage coupled with CFPPs attracted extensive attention because it could partially decouple heat production from electricity generation. Molten-salt thermal storage was one of the most widely studied options due to its high heat capacity, low storage cost, and mature engineering experience (Liu *et al.* 2025; Zhang *et al.* 2022a; Bauer *et al.* 2013; Zhang *et al.* 2022b). Previous studies demonstrated that thermal storage integration could significantly reduce the minimum technical output of CFPPs and enhance peak-shaving capability (Liu *et al.* 2025; Zhang *et al.* 2022a). However, direct thermal storage often suffered from heat-source and storage-temperature mismatches, leading to exergy destruction and limiting the utilization efficiency of thermal energy (Wang *et al.* 2025; Yan *et al.* 2026).

Heat pump energy storage (HPES), also known as a Carnot battery, emerged as a promising solution for converting electricity into thermal energy and recovering it when needed (Vecchi *et al.* 2022; Dumont *et al.* 2020; Novotny *et al.* 2022). Compared with direct electric heating, HPES could achieve a higher round-trip efficiency (RTE) by upgrading low-grade heat to a higher temperature level. In particular, CO_2 heat pumps attracted increasing interest because CO_2 was environmentally friendly and exhibited favorable heat-transfer characteristics under transcritical conditions, enabling effective temperature matching with sensible thermal storage media (Adamson *et al.* 2022; Aga *et al.* 2016; Shamsi *et al.* 2024). Therefore, integrating CO_2 heat pumps with CFPPs provided a promising pathway for enhancing flexibility and accommodating surplus renewable electricity.

However, most existing studies employed direct coupling between the heat pump and the CFPP. In such configurations, the operation of the heat pump relied on the instantaneous availability of extraction steam, exhaust steam, or flue-gas heat from the power plant. Consequently, the charging process remained strongly constrained by the operating state of the CFPP, limiting the ability of the storage system to respond independently to fluctuating renewable-electricity availability. A decoupled configuration was therefore desirable, in which low-grade heat from the CFPP was first stored in an intermediate thermal storage unit, allowing the CO_2 heat pump to operate independently according to renewable-electricity availability rather than the real-time load condition of the power plant.

To address the intermittency of wind and solar energy, and improve the renewable energy accommodation capability of CFPP-based power systems, a CO_2 HPES system decoupled from a CFPP was proposed in this work. In the proposed system, low-pressure extraction steam was used to store heat in a low-temperature water tank. This low-temperature thermal storage unit acted as an intermediate heat buffer between the CFPP and the CO_2 heat pump. Based on the proposed decoupled configuration, a thermodynamic model was established to evaluate the performance of the integrated system under variable CFPP loads, and the thermodynamic characteristics and key design parameters were investigated.

2. System description

To retrofit existing CFPPs for deep peak-shaving operation, a decoupled CO_2 HPES system was proposed, as illustrated in Figure 1. The boundary conditions and component parameters of the CFPP model were obtained from the design data of a 600 MW supercritical unit at Zhuanghe Power Plant in Dalian, China. The proposed system consisted of four main subsystems: the original CFPP, a steam-extraction thermal storage subsystem, a CO_2 heat pump subsystem, and a molten-salt thermal storage subsystem. By introducing an intermediate low-temperature water-storage subsystem between the CFPP and the CO_2 heat pump, the operation of the heat pump was decoupled from the

instantaneous operating condition of the power plant, enabling flexible utilization of surplus electricity from both renewable energy and the CFPP.

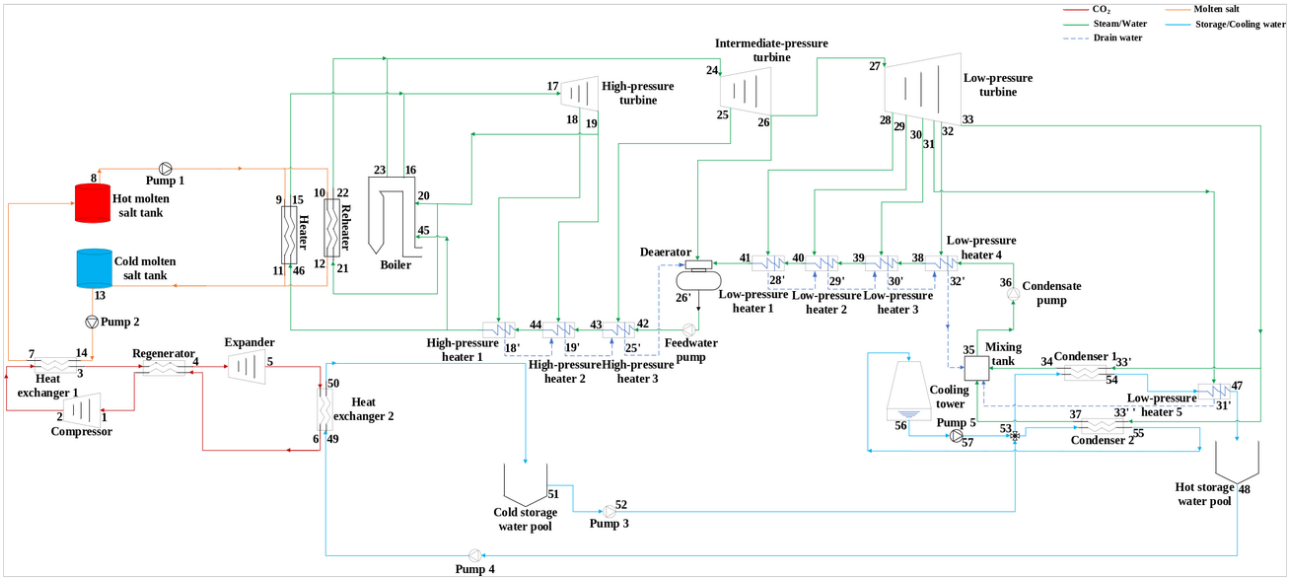

Figure 1. Schematic diagram of a CO_2 heat pump thermal storage system decoupled from a CFPP.

In the steam-extraction thermal storage subsystem, part of the fifth-stage low-pressure extraction steam was diverted from the regenerative system to heat storage water. The heated water was stored in dedicated water tanks and served as an intermediate low-temperature thermal reservoir. Compared with conventional directly coupled configurations, this arrangement allowed low-grade thermal energy from the CFPP to be stored independently and utilized by the heat pump when electricity was available, thereby reducing the dependence of the charging process on the real-time operating condition of the power plant. The CO_2 heat pump upgraded the stored low-temperature thermal energy to a higher temperature level and transferred it to the molten-salt thermal storage subsystem. Owing to the favorable temperature-matching characteristics of transcritical CO_2 heat pumps, efficient heat transfer between the storage water and molten salt could be achieved. The molten salt acted as the high-temperature thermal storage medium and provided the thermal energy required during the discharging process.

The integrated system operated in three periods: charging, normal-operation, and discharging modes. During the charging process, the CFPP operated at a low load, typically 30% turbine heat acceptance (THA), and low-grade heat from the fifth-stage extraction steam was first stored in the water-storage subsystem. The stored heat was then upgraded by the CO_2 heat pump and transferred to the molten-salt thermal storage system using surplus electricity. During normal operation, the CFPP operated flexibly under conventional regenerative conditions. During the discharging process, the thermal energy stored in the molten-salt tanks was released to heat the feedwater and reheat steam, generating additional superheated steam and increasing the turbine output during peak-demand periods. In this way, the proposed system enhanced the operational flexibility and peak-shaving capability of the CFPP while improving the utilization of surplus renewable electricity.

Owing to the proposed decoupled configuration, three low-load power regulation modes could be realized. In Mode 1, only the steam extraction thermal storage subsystem operated, and low-pressure extraction steam was used to charge the water storage subsystem for deep peak shaving. In Mode 2, only the CO_2 heat pump operated using surplus CFPP electricity or renewable energy to upgrade low-temperature stored heat into high-temperature thermal energy in the molten salt storage system. In Mode 3, the steam extraction subsystem and the CO_2 heat pump operated simultaneously, combining steam extraction and electrical energy consumption to maximize the charging capability. These

operating modes significantly improved the flexibility of the proposed system under different grid regulation and renewable energy accommodation scenarios.

3. Thermodynamic modeling

The thermodynamic model was developed under steady-state conditions. Changes in kinetic and potential energies were neglected, and all heat exchangers were assumed to operate in counter-current flow. The turbine, CO_2 compressor, expander, and pumps were modelled using specified isentropic efficiencies. Pressure drops in pipes and heat exchangers were neglected; therefore, the pressure at the outlet of each heat exchanger was assumed to be equal to that at the corresponding inlet. Heat losses from pipes, heat exchangers, water-storage tanks, and molten-salt tanks were neglected in the base-case calculation.

3.1. Energy model

CFPP

For the high-pressure heaters (HPHs), the MTBE-based thermal balance formula was shown as Eq. (1) (Hou *et al.* 2024):

$$\begin{bmatrix} q_1 & & & \\ \gamma_2 & q_2 & & \\ \gamma_3 & \gamma_3 & q_3 & \\ \gamma_4 & \gamma_4 & \gamma_4 & q_4 \end{bmatrix} \begin{bmatrix} m_1 \\ m_2 \\ m_3 \\ m_4 \end{bmatrix} = m_{fwh} \begin{bmatrix} \tau_1 \\ \tau_2 \\ \tau_3 \\ \tau_4 \end{bmatrix} \tag{1}$$

For the low-pressure heaters (LPHs), the MTBE-based thermal balance formula was shown as Eq. (2):

$$\begin{bmatrix} q_5 & & & \\ \gamma_6 & q_6 & & \\ \gamma_7 & \gamma_7 & q_7 & \\ \gamma_8 & \gamma_8 & \gamma_8 & q_8 \end{bmatrix} \begin{bmatrix} m_5 \\ m_6 \\ m_7 \\ m_8 \end{bmatrix} = m_{fwl} \begin{bmatrix} \tau_5 \\ \tau_6 \\ \tau_7 \\ \tau_8 \end{bmatrix} \tag{2}$$

Where:

- m_i (i=1~8) = mass flow rate of the i-th extraction steam (kg/s);
- γ_i (i=1~8) = drain enthalpy drop of the i-th feedwater heater (kJ/kg);
- τ_i (i=1~8) = feedwater enthalpy rise of the i-th feedwater heater (kJ/kg);
- q_i (i=1~8) = heat released by extraction steam in the i-th feedwater heater (kJ/kg);
- m_{fwh} = mass flow rate of feedwater in HPHs (kg/s);
- m_{fwl} = mass flow rate of feedwater in low-pressure feedwater heaters (LPHs) (kg/s).

For each surface-type feedwater heater except the deaerator, the required parameters γ_i, τ_i, and q_i were defined as Eq. (3):

$$\begin{cases} \gamma_i = h_{d(i-1)} - h_{di} \\ \tau_i = h_{fwi} - h_{fw(i+1)} \\ q_i = h_{ei} - h_{di} \end{cases} \tag{3}$$

Where:

- $h_{d(i-1)}$ = inlet specific enthalpy of drain water in the i-th feedwater heater (kJ/kg);
- h_{di} = outlet specific enthalpy of drain water in the i-th feedwater heater (kJ/kg);
- h_{ei} = specific enthalpy of the i-th extraction steam (kJ/kg);

- $h_{fw(i+1)}$ = inlet specific enthalpy of feedwater in the i-th feedwater heater (kJ/kg);
- h_{fwi} = outlet specific enthalpy of feedwater in the i-th feedwater heater (kJ/kg).

For the deaerator, the corresponding expressions for γ_i, τ_i, and q_i were defined by Eq. (4):

$$\begin{cases} \gamma_4 = h_{d3} - h_{fw5} \\ \tau_4 = h_{fw4} - h_{fw5} \\ q_4 = h_{e4} - h_{fw5} \end{cases} \tag{4}$$

Based on the mass and energy balance equations, the turbine power output P_{tur}, boiler heat input Q_b, and net power output of the integrated system P_{net} could be calculated.

Additionally, for the turbine-generator unit operating under off-design conditions, the relationship between steam parameters and mass flow rates satisfied the Flügel formula, which was expressed as Eq. (5):

$$\frac{m_{var}}{m_{ref}} = \sqrt{\frac{p_{in,var}^2 - p_{out,var}^2}{p_{in,ref}^2 - p_{out,ref}^2}} \frac{\sqrt{T_{in,ref}}}{\sqrt{T_{in,var}}} \tag{5}$$

Where:

- $p_{in,ref}$, $p_{out,ref}$, $T_{in,ref}$, m_{ref} = turbine inlet pressure (kPa), outlet pressure (kPa), inlet temperature (K), and mass flow rate (kg/s) under reference operating condition, respectively;
- $p_{in,var}$, $p_{out,var}$, $T_{in,var}$, m_{var} = turbine inlet pressure (kPa), outlet pressure (kPa), inlet temperature (K), and mass flow rate (kg/s) under off-design condition, respectively.

Based on the above CFPP model, the steam-extraction thermal storage subsystem was further modeled using the corresponding mass and energy balances. During charging, Pump 3 circulated the storage water through the steam–water heat exchanger. Its electricity consumption was calculated as Eq. (6):

$$W_{p3} = m_{sw,CFPP} Hg / \eta_{ps} / \eta_m / \eta_g \tag{6}$$

Where:

- $m_{sw,CFPP}$ = mass flow rate of storage water during steam-extraction thermal storage (kg/s);
- H= head of pumps (m);
- g = gravitational acceleration (m/s^2);
- η_{ps}= isentropic efficiency of pumps;
- η_m= mechanical efficiency;
- η_g = generator efficiency.

CO_2 heat pump

The energy balance equations for key components of the CO_2 heat pump were summarized in Table 1. During system operation, both molten salt and storage water exchanged heat with CO_2. Accordingly, the circulation pumps supporting the operation, namely Pump 2 and Pump 4, were also mathematically modeled and presented in Table 1.

Table 1. Energy balance equations for each component of the CO_2 heat pump.

Component	Equation
Compressor	$W_{com} = \dot{m}_{CO_2}(h_2 - h_1) = \dot{m}_{CO_2}(h_{2s} - h_1)/\eta_{cs}/\eta_m/\eta_g$
Heat exchanger 1	$Q_{he1} = \dot{m}_{CO_2}(h_2 - h_3) = \dot{m}_{ms,\,cold} c_{ms}(T_7 - T_{14})$
Heat exchanger 2	$Q_{he2} = \dot{m}_{CO_2}(h_6 - h_5) = \dot{m}_{sw,\,hot}(h_{49} - h_{50})$
Regenerator	$Q_{regen} = \dot{m}_{CO_2,\,hot}(h_3 - h_4) = \dot{m}_{CO_2,\,cold}(h_1 - h_6)$
Expander	$W_{\exp} = \dot{m}_{CO_2}(h_4 - h_5) = \dot{m}_{CO_2}(h_4 - h_{5s})\eta_{exs}\eta_m\eta_g$
Pump 2	$W_{p2} = m_{ms,\,cold} Hg/\eta_{ps}/\eta_m/\eta_g$
Pump 4	$W_{p4} = m_{sw,\,hot} Hg/\eta_{ps}/\eta_m/\eta_g$

For the compressor, the isentropic outlet state 2s was first determined from p_2 and s_{2s}=s_1. The actual outlet enthalpy was then calculated using the compressor isentropic efficiency, as shown in Eq. (7):

$$\eta_{cs} = \frac{h_{2s} - h_1}{h_2 - h_1} \tag{7}$$

For the expander, the isentropic outlet state 5s was determined from p_5 and s_{5s}=s_4, and the actual outlet enthalpy was obtained from Eq. (8):

$$\eta_{exs} = \frac{h_4 - h_5}{h_4 - h_{5s}} \tag{8}$$

The compressor electricity consumption and expander electricity generation were further corrected using the mechanical and generator efficiencies. The design isentropic efficiencies of the compressor and expander were 0.85 and 0.87, respectively, while both the mechanical and generator efficiencies were 0.98.

To evaluate the local temperature differences, each counter-current heat exchanger was discretised into 100 control volumes, and the temperature profiles of the hot and cold streams were calculated along the heat-transfer direction.

3.2. Performance indicators

Based on the component energy balance equations in Table 1, coefficient of performance (COP) of the heat pump could be expressed as Eq. (9):

$$COP = \frac{Q_{he1}}{W_{com} - W_{\exp}} \tag{9}$$

The overall gross power generation efficiency of the CFPP was defined as the ratio of the turbine power output to the total heat input to the boiler, as expressed by Eq. (10):

$$\eta_{gen} = \frac{P_{tur}}{Q_b} \times 100\% \tag{10}$$

Where:

- P_{tur} = total power output of turbine (MW);
- Q_b = heat input of the boiler (MW);

During the low-load charging phase, the turbine power output was reduced by steam extraction and heat-pump operation, and the minimum achievable load ratio could be expressed as Eq. (11) and Eq. (12):

$$P_{low} = \lambda_{CFPP} \times P_{rated} - \left(P_{LPH5,loss} + W_{p3} + W_{com} + W_{p4} + W_{p2} - W_{exp}\right) \tag{11}$$

$$\lambda_{\min,es} = \frac{P_{low}}{P_{rated}} \tag{12}$$

During the high-load discharging phase, the power output was increased by the additional generation from the molten-salt storage system, and the maximum achievable load ratio was expressed by Eq. (13):

$$\lambda_{max,es} = \frac{P_{high}}{P_{rated}} = \frac{\lambda_{CFPP} \times P_{rated} + \Delta P_{net}}{P_{rated}} \tag{13}$$

Where:

- P_{low} = net external power output of the integrated system under the minimum-load condition (MW);
- λ_{CFPP} = load ratio of standalone CFPP without energy storage, ranging from 30% to 100%;
- P_{rated} = rated power capacity of the CFPP (MW);
- $P_{LPH5,loss}$ = power loss induced by the fifth-stage extraction steam (MW);
- W_{p4}, W_{p2} = power consumption of water pump and molten salt pump (MW), respectively;
- $\lambda_{min,es}$, $\lambda_{max,es}$ = minimum and maximum achievable external power supply ratios of the CFPP integrated with energy storage system, respectively;
- ΔP_{net} = incremental net power output during discharge after deducting all additional auxiliary power consumption associated with the molten-salt thermal energy storage system (MW).

To evaluate the overall performance of the integrated thermal energy storage system, the RTE boundary included the steam-extraction thermal storage subsystem, the CO_2 heat pump, the water and molten-salt circulation pumps, and the additional power-generation process during discharge. The charging energy included the equivalent power loss caused by fifth-stage steam extraction, the net electricity consumption of the CO_2 heat pump, and the associated pump consumption. The discharge energy was defined as the incremental net electricity output relative to the standalone CFPP at the same baseline THA load. Heat losses from the storage tanks and pipelines were neglected under the steady-state adiabatic assumption, as expressed in Eq. (14), (15) and (16).

$$E_{char} = \left(P_{LPH5,loss} + W_{p3}\right) \times t_{ex} + \left(W_{com} - W_{exp} + W_{p4} + W_{p2}\right) \times t_{hp} \tag{14}$$

$$E_{dis} = \Delta P_{net} \times t_{ms} \tag{15}$$

$$RTE = \frac{E_{dis}}{E_{char}} \tag{16}$$

Where:

- E_{char} = energy consumption in the charging process (MWh);
- E_{dis} = total net electricity output in the discharging process (MWh);
- t_{ex} = extraction heat storage hours (h);
- t_{hp} = heat pump operation hours (h);
- t_{ms} = molten salt generation hours (h).

4. Working conditions

The detailed design conditions were summarized in Table 2. It should be noted that the thermophysical properties of CO_2 and water were evaluated using REFPROP through a MATLAB interface. Enthalpy, entropy, density, and specific heat capacity were calculated as functions of temperature and pressure at each state point. The CO_2 compressor and expander outlet states were determined from the corresponding isentropic reference states and the specified isentropic efficiencies. The REFPROP reference-state convention was used consistently throughout the calculation. In addition, solar salt consisting of 60% $NaNO_3$ and 40% KNO_3 was adopted as the high-temperature storage medium. Its density and specific heat capacity were calculated using the temperature-dependent correlations reported by D'Aguanno *et al.* (2018). In the following correlations, T is expressed in K, ρ in kg/m^3, and c_p in J/(kg·K).

Table 2. Thermodynamic and operational design parameters of the system.

Category	Parameter	Value
CFPP	Geographic position	38.9°N; 121.6°E
	Rated power output / MW	600
	Boiler feedwater temperature / °C	275
	Boiler feedwater pressure / MPa	28.87
	Boiler efficiency / %	93.83
	Mechanical efficiency η_m / %	98
	Generator efficiency η_g / %	98
	Isentropic efficiency of pumps η_{ps} / %	85
	Inlet steam temperature of HPT and IPT / °C	566
	Inlet pressure of HPT / MPa	24.2
	Inlet pressure of IPT / MPa	3.81
Extraction steam and heat storage subsystem	Extraction heat storage hours t_{ex} / h	8
	Low-pressure 5th extraction steam ratio / %	5
	Low-pressure 5th extraction steam saturation temperature / °C	72
	Hot storage water pool temperature / °C	70
	Hot storage water pool pressure / MPa	1
	Cold storage water pool temperature / °C	10
CO_2 heat pump	Heat pump operation hours t_{hp} / h	8
	Compressor inlet temperature / °C	400
	Compressor inlet pressure / MPa	2
	Isentropic efficiency of compressor / %	85
	Isentropic efficiency of CO_2 expander / %	87
	Hot molten salt tank temperature / °C	580
	Cold molten salt tank temperature / °C	320
	Molten salt generation hours t_{ms} / h	5

Table 2. (continued)

Category	Parameter	Value
Property of molten salt (D'Aguanno *et al.* 2018)	Density / kg/m³	$\rho = 2090 - 0.636 \times T$
	Specific heat capacity / J/(kg·K)	$c_p = 1443 + 0.172 \times T$

5. Results and discussion

Based on the reference-condition parameters, the thermodynamic and peak-shaving performances of the proposed system were evaluated. The charging process was performed at 30% THA, while the discharging process was analyzed under 30%, 50%, 75%, and 100% THA operating conditions. Key performance indicators, including power output, peak-shaving capability, RTE, and coal consumption rate, were calculated and compared. Since THA was widely adopted in power plant engineering to represent unit load levels relative to the rated condition, it was used throughout the following analysis.

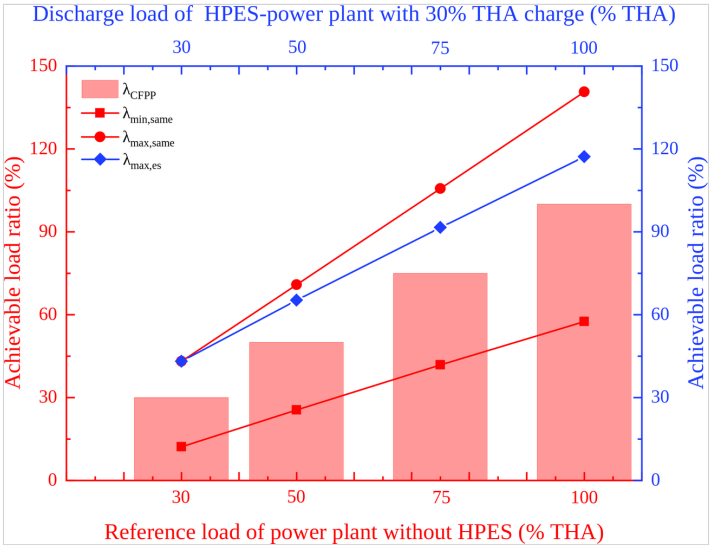

Figure 2. Peak-shaving performance of the HPES-power plant under different charging and discharging conditions.

As shown in Figure 2, the peak-shaving performance of the HPES-power plant was evaluated under different charging and discharging conditions. The red bars denoted the reference load under matched charging and discharging conditions, where both charging and discharging were performed at the same THA load. This reference case served as a benchmark to quantify the improvement in peak-shaving capability achieved by the proposed operation strategy under mismatched charging and discharging conditions. The red line indicated the maximum and minimum peak-shaving capability achievable under these matched operating conditions. The minimum load shown by the red line corresponded to Mode 3 operation, in which steam extraction and heat pump charging were simultaneously employed, thereby providing the strongest peak-shaving capability among the three charging modes. In contrast, the blue line represented the maximum achievable peak-shaving load under a fixed charging load of 30% THA, with discharging loads of 30%, 50%, 75%, and 100% THA. Additionally, under the 30% THA charging scenario, η_{gen} ranged from 33.98% to 45.15%, and the RTE ranged from 44.29% to 58.09%.

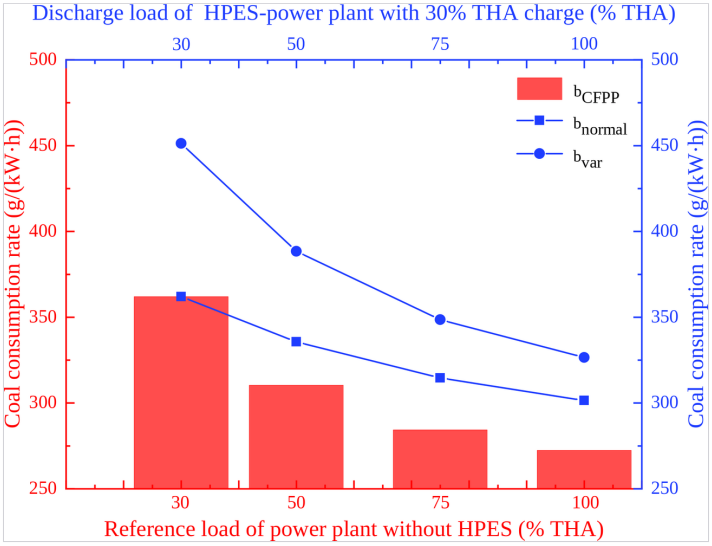

Figure 3. Coal consumption rates of the power plant under different charging and discharging conditions.

As shown in Figure 3, the coal consumption rates of the HPES-power plant under different operating conditions were further analyzed. The red bars represented the coal consumption rates under matched charging and discharging loads, while the line denoted by bnormal corresponded to the coal consumption rate under a fixed 30% THA charging condition with different discharging loads, when peak-shaving operation was not considered. Additionally, the line denoted by bvar represented the coal consumption rate when peak-shaving operation was considered under the same charging condition.

From Figure 3, it could be observed that compared with the normal operating condition, the coal consumption rate was higher under peak-shaving operation. Nevertheless, the system still maintained acceptable thermodynamic performance under the 30% THA charging scenario while providing considerable peak-shaving capability. Combined with the results presented in Figure 2, this demonstrated the necessity and practical feasibility of adopting the 30% THA charging condition. Therefore, the subsequent reference-condition analyses were carried out based on the 30% THA charging case, with the 50% THA discharging condition selected as the reference operating case. This choice was motivated by the fact that CFPPs generally operated around a medium-load level during long-term operation, making 50% THA a representative condition for assessing the performance of the proposed system.

Table 3 presented the thermodynamic performance of the system under the reference condition of 30% THA charging and 50% THA discharging. During the charging process, the steam extraction thermal storage subsystem and the CO_2 heat pump operated simultaneously (Mode 3), representing the maximum charging capacity scenario considered in this study. Under this condition, the system achieved a COP of 1.32 and an RTE of 53.41%, while the generation efficiency reached 39.62%. In addition, the coal consumption rates under normal and peak-shaving conditions were 335.66 g/(kW·h) and 388.36 g/(kW·h), respectively. The corresponding molten salt and water storage capacities were also summarized in the table, providing a quantitative description of the storage requirements under the reference operating condition.

Table 3. Thermodynamic performance of the system under reference operating condition.

Parameter	Value
COP	1.32
RTE / %	53.41
η_{gen} / %	39.62

Table 3. (continued)

Parameter	Value
$\lambda_{min,es}$ of Mode 1 / %	29.72
$\lambda_{min,es}$ of Mode 2 / %	12.44
$\lambda_{min,es}$ of Mode 3 / %	12.16
$\lambda_{max,es}$ / %	65.24
b_{normal} / g/(kW·h)	335.66
b_{var} / g/(kW·h)	388.36
M_{ms} / t	1.02×10^4
$V_{ms,total}$ / m^3	5.68×10^3
M_{sw} / t	3.82×10^3
$V_{sw,total}$ / m^3	7.73×10^3

Furthermore, under the reference operating condition, the calculated minimum approach temperature differences of heat exchanger 1, heat exchanger 2, and the regenerator were 19.0, 10.0, and 18.5 K, respectively. No internal temperature crossover occurred in any of the heat exchangers.

6. Conclusion

To address the intermittency of renewable energy and enhance the flexibility and peak-shaving capability of CFPPs, a CO_2 HPES system decoupled from a CFPP was proposed in this study. The charging and discharging processes were effectively decoupled through a storage water subsystem, enabling flexible energy management and independent operation of the heat pump and power generation units.

Based on the established thermodynamic models, the performance of the proposed system under the reference operating condition was investigated. The results showed that, under the reference operating conditions of 30% THA charging and 50% THA discharging, the CO_2 heat pump achieved a COP of 1.32, while the overall system attained an RTE of 53.41%. The corresponding minimum and maximum peak-shaving load ratios were 12.16% and 65.24%, respectively, demonstrating the capability of the proposed system to significantly enhance the operational flexibility of the CFPP. When peak-shaving operation was considered, the coal consumption rate was 388.36 g/(kW·h). In addition, the required volumes of the molten salt storage tanks and storage water pools were 5.68×10^3 m^3 and 7.73×10^3 m^3, respectively. These results indicated that the proposed system could effectively achieve deep peak shaving while maintaining favorable thermodynamic performance, providing a promising solution for enhancing CFPP flexibility and accommodating renewable energy.

Although the proposed system demonstrated promising thermodynamic performance, several limitations remained. First, the thermodynamic model was developed under steady-state conditions with several simplifying assumptions, including negligible pressure drops and heat losses. Although the CFPP boundary conditions and component parameters were obtained from the design data of the reference plant, comprehensive validation against multi-load operational data was not conducted because such data were unavailable for the present study. In addition, the dynamic operating characteristics and control strategies of the system under actual grid fluctuations, as well as its coupling with variable renewable energy sources, were not fully considered. Future work will therefore focus on validation using measured plant data, dynamic simulation, operating-strategy optimisation, and the integration of the proposed system with large-scale renewable energy to further improve its flexibility, stability, and practical applicability.

Declarations

Author contributions. Tengjiao Jia: Writing (original draft), Methodology, Investigation, Formal analysis, Conceptualization. Wen Su: Funding acquisition, Writing (review and editing), Validation, Methodology, Conceptualization, Supervision. Xinxing Lin: Writing (review and editing), Validation, Methodology, Conceptualization. Zhimei Zheng: Supervision, Methodology.

Funding. The authors would like to acknowledge the funding support by the Key R&D Project of Hunan Province (2025WK2007).

Awards. Department of Science and Technology of Hunan Province (2025WK2007)

Conflicts of interest. The authors declare no competing interests.

Data availability. Not applicable. This study did not generate or analyse any datasets.

References

Adamson, Keri-Marie; Walmsley, Timothy Gordon; Carson, James K.; Chen, Qun; Schlosser, Florian; Kong, Lana; Cleland, Donald John (2022) 'High-temperature and transcritical heat pump cycles and advancements: A review', *Renewable and Sustainable Energy Reviews*, 167, pp. 112798. Available at: https://doi.org/10.1016/j.rser.2022.112798

Aga, Vipluv; Conte, Enrico; Carroni, Richard; Burcker, Bertrand; Ramond, Mathieu (2016) 'Supercritical CO2-based heat pump cycle for electrical energy storage for utility scale dispatchable renewable energy power plants', *Proceedings of the 5th International Symposium on Supercritical CO2 Power Cycles, San Antonio, Texas*. Available at: https://www.sco2symposium.com/papers2016/Thermal/094paper.pdf

Bauer, Thomas; Pfleger, Nicole; Laing, Doerte; Steinmann, Wolf-Dieter; Eck, Markus; Kaesche, Stefanie (2013) 'High-Temperature Molten Salts for Solar Power Application', *Molten Salts Chemistry*. Elsevier, pp. 415-438. Available at: https://doi.org/10.1016/b978-0-12-398538-5.00020-2

D'Aguanno, B.; Karthik, M.; Grace, A. N.; Floris, A. (2018) 'Thermostatic properties of nitrate molten salts and their solar and eutectic mixtures', *Scientific Reports*, 8(1). Available at: https://doi.org/10.1038/s41598-018-28641-1

Dumont, Olivier; Frate, Guido Francesco; Pillai, Aditya; Lecompte, Steven; De paepe, Michel; Lemort, Vincent (2020) 'Carnot battery technology: A state-of-the-art review', *Journal of Energy Storage*, 32, pp. 101756. Available at: https://doi.org/10.1016/j.est.2020.101756

Dunn, Bruce; Kamath, Haresh; Tarascon, Jean-Marie (2011) 'Electrical Energy Storage for the Grid: A Battery of Choices', *Science*, 334(6058), pp. 928-935. Available at: https://doi.org/10.1126/science.1212741

Fang, Fang; Sun, Yutong; Zhang, Yi; Du, Ming; Liu, Jizhen (2025) 'Dynamic modeling and performance analysis of a coal-fired power plant integrated with flue gas-molten salt thermal energy storage system', *Applied Thermal Engineering*, 280, pp. 128348. Available at: https://doi.org/10.1016/j.applthermaleng.2025.128348

Hou, Kun; Wang, Yan; Han, Ningze; Ma, Tingshan; Lv, Kai; Liu, Xiangyang; He, Maogang (2024) 'Performance analysis of a liquid carbon dioxide energy storage system integrated with a coal-fired power plant', *Journal of Energy Storage*, 77, pp. 109869. Available at: https://doi.org/10.1016/j.est.2023.109869

International Energy Agency (2024a) *Electricity 2024: Analysis and Forecast to 2026*. Available at: https://www.iea.org/reports/electricity-2024

International Energy Agency (2024b) *Renewables 2024: Analysis and Forecast to 2030*. Available at: https://www.iea.org/reports/renewables-2024

Liu, Ming; Miao, Lin; Wang, Zhu; Yan, Junjie (2025) 'Design and thermo-economic analysis on molten salt thermal energy storage system integrated within coal-fired power plant: Co-storing energy from live and reheat steam', *Journal of Energy Storage*, 131, pp. 117637. Available at: https://doi.org/10.1016/j.est.2025.117637

Luo, Xing; Wang, Jihong; Dooner, Mark; Clarke, Jonathan (2015) 'Overview of current development in electrical energy storage technologies and the application potential in power system operation', *Applied Energy*, 137, pp. 511-536. Available at: https://doi.org/10.1016/j.apenergy.2014.09.081

Novotny, Vaclav; Basta, Vit; Smola, Petr; Spale, Jan (2022) 'Review of Carnot Battery Technology Commercial Development', *Energies*, 15(2), pp. 647. Available at: https://doi.org/10.3390/en15020647

Richter, Marcel; Oeljeklaus, Gerd; Görner, Klaus (2019) 'Improving the load flexibility of coal-fired power plants by the integration of a thermal energy storage', *Applied Energy*, 236, pp. 607-621. Available at: https://doi.org/10.1016/j.apenergy.2018.11.099

Shamsi, Syed Safeer Mehdi; Barberis, Stefano; Maccarini, Simone; Traverso, Alberto (2024) 'Large scale energy storage systems based on carbon dioxide thermal cycles: A critical review', *Renewable and Sustainable Energy Reviews*, 192, pp. 114245. Available at: https://doi.org/10.1016/j.rser.2023.114245

Vecchi, Andrea; Knobloch, Kai; Liang, Ting; Kildahl, Harriet; Sciacovelli, Adriano; Engelbrecht, Kurt; Li, Yongliang; Ding, Yulong (2022) 'Carnot Battery development: A review on system performance, applications and commercial state-of-the-art', *Journal of Energy Storage*, 55, pp. 105782. Available at: https://doi.org/10.1016/j.est.2022.105782

Wang, Yuanjing; Gong, Liangyong; Zhang, Yanping (2025) 'Peak shaving performance analysis of a coal-fired power plant integrated with molten salt thermal energy storage system based on energy-potential matching principle', *Journal of Energy Storage*, 124, pp. 116956. Available at: https://doi.org/10.1016/j.est.2025.116956

Xu, Qilong; Wang, Shuai; Luo, Kun; Fan, Jianren (2025) 'Energy-saving retrofit and thermal economy optimization of peak-shaving for coal-fired power plants utilizing molten salt thermal storage', *Applied Thermal Engineering*, 280, pp. 128229. Available at: https://doi.org/10.1016/j.applthermaleng.2025.128229

Yan, Zhiyuan; Tan, Rui; Meng, Fanxing; Jiang, Guo'an; Ren, Fengying; He, Xinrong; Zhang, Tao; Ren, Xiaohan (2026) 'Molten-Salt-Based Thermal Storage for Thermal Power Plant Peaking', *Energies*, 19(5), pp. 1246. Available at: https://doi.org/10.3390/en19051246

Zhang, Kezhen; Liu, Ming; Zhao, Yongliang; Yan, Hui; Yan, Junjie (2022a) 'Design and performance evaluation of a new thermal energy storage system integrated within a coal-fired power plant', *Journal of Energy Storage*, 50, pp. 104335. Available at: https://doi.org/10.1016/j.est.2022.104335

Zhang, Kezhen; Liu, Ming; Zhao, Yongliang; Zhang, Shunqi; Yan, Hui; Yan, Junjie (2022b) 'Thermo-economic optimization of the thermal energy storage system extracting heat from the reheat steam for coal-fired power plants', *Applied Thermal Engineering*, 215, pp. 119008. Available at: https://doi.org/10.1016/j.applthermaleng.2022.119008

HOW TO CITE THIS PAPER

Jia, T., Su, W., Lin, X. and Zheng, Z. (2026). Design and performance analysis of a CO_2 heat pump thermal storage system decoupled from a coal-fired power plant. In: *Proceedings of the 22nd International Conference on Sustainable Energy Technologies (SET2026)*, Kuala Lumpur, Malaysia, 13 to 15 August 2026. Caravel Press, pp. 69–81. ISBN 978-1-995850-00-9. ISSN 2978-4387. https://doi.org/10.65582/set.2026.006

COPYRIGHT AND LICENCE

© 2026 The Author(s). This is an open access paper distributed under the terms of the Creative Commons Attribution (CC BY 4.0) licence, which permits unrestricted use, distribution and reproduction in any medium, provided the original work is properly cited.

WSSET World Society of Sustainable Energy Technologies Organised by the World Society of Sustainable Energy Technologies. Published by Caravel Press.